Characteristics of aerosol pollution during heavy haze events in Suzhou, China

Mi Tian[1], Huanbo Wang[1], Yang Chen[1], Fumo Yang[1,2,3*], Xiaohua zhang[4], Qiang Zou[4], Renquan Zhang[4], Yongliang Ma[5], Kebin He[5]

[1]Key Laboratory of Reservoir Aquatic Environment of CAS, Chongqing Institute of Green and Intelligent Technology, Chinese Academy of Sciences, Chongqing 400714, China

[2]Center for Excellence in Urban Atmospheric Environment, Institute of Urban Environment, Chinese Academy of Sciences, Xiamen 361021, China

[3]Changjiang Normal University, Chongqing 408100, China.

[4]Suzhou Environmental Monitoring Center, Suzhou 215004, China

[5]School of Environment, Tsinghua University, Beijing 100012, China

Correspondence to: F. M. Yang (fmyang@cigit.ac.cn)

Abstract

Extremely severe haze weather events occurred in many cities in China, especially in the east part of the country, in January 2013. Comprehensive measurements including hourly concentrations of $PM_{2.5}$ and its major chemical components (water-soluble inorganic ions, OC, and EC) and related gas-phase precursors were conducted via on-line monitoring system in Suzhou, a medium size city of Jiangsu province, just east of Shanghai. $PM_{2.5}$ frequently exceeded 150 μg m^{-3} on hazy days, with the maximum reaching 324 μg m^{-3} on Jan. 14, 2013. Unfavorable weather conditions (high RH, and low rainfall, wind speed and atmospheric pressure) were conducive for the haze formation. High concentrations of secondary aerosol species (including SO_4^{2-}, NO_3^-, NH_4^+, and SOC) and gaseous precursors were observed during the first two haze events, while elevated primary carbonaceous species emissions were found during the third haze period, pointing to different haze formation mechanisms. OM, $(NH_4)_2SO_4$, NH_4NO_3 were found to be the major contributors to visibility impairment. High concentrations of sulfate and nitrate might be explained by homogeneous gas-phase reactions under low RH conditions and by heterogeneous processes under relatively high RH conditions. Analysis of air mass trajectory clustering and potential source contribution function manifested that aerosol pollutions in the studied areas were mainly caused by local activities and surrounding sources transported from nearby cities.

1. Introduction

Haze is defined as visibility lower than 10 km when relative humidity < 80%. Rapidly increased air pollution in China in the past several decades have resulted in frequent occurrences of haze events, which have caused great concern to the scientific community as well as the public (Zhang et al., 2012). Haze events have adverse effects on human health, traffic, climate, and other important aspects (Zhang et al., 2015; Charlson et al., 1987; Ramanathan and Vogelmann, 1997; Tegen et al., 2000; Yu et al., 2002; Tie et al., 2009a; Tie et al., 2009b). Fine particles ($PM_{2.5}$, aerosols with an

aerodynamic diameter of 2.5 microns or less) are largely responsible for haze formation due to their ability in light extinction including scattering and absorbing solar and infrared radiation (Yu et al., 2014). Light extinction of $PM_{2.5}$ is highly associated with its chemical composition (Tao et al., 2014). Water-soluble inorganic ions and carbonaceous species often account for major fractions of $PM_{2.5}$ and are important contributors to visibility impairment (Tan et al., 2009; Pathak et al., 2009), and thus have been investigated extensively (Yang et al., 2005; Jansen et al., 2014; Pathak et al., 2009). Most existing studies were based on filter sampling and off-line analysis and had limitations in providing detailed insight into the roles the major chemical species played during shorter haze periods.

High contributions of secondary inorganic aerosols (SIA, including sulfate, nitrate and ammonium), the predominant water-soluble ionic species in $PM_{2.5}$, to visibility reduction have been observed in many cities in China (Huang et al., 2014). Gas- or liquid-phase reactions of sulfur dioxide and nitrogen oxides are the primary mechanisms forming aerosol sulfate and nitrate. For the formation of sulfate, homogeneous gas phase reaction of SO_2 with OH radical, and heterogeneous reactions in the aqueous surface layer of pre-existing particles and in-cloud processes are the primary mechanisms (Wang et al., 2006). The rates of gas-phase and liquid-phase reactions of SO_2 were similar in summer while the heterogeneous processes were responsible for the oxidation in winter (Hewitt, 2001). Nitric acid can be formed from homogeneous gas-phase reactions of NO_2 with OH or O_3 and from heterogeneous hydrolysis of N_2O_5, which occurred predominantly during daytime and nighttime, respectively (Khoder, 2002). Both sulfuric acid and nitric acid react with alkaline substance in the atmosphere, mostly ammonia under ambient conditions to produce salts (Hewitt, 2001). The neutralization of sulfuric acid by ammonia has been found to be preferred over the formation of ammonium nitrate (Warneck, 1999). Thus, the formation of ammonium nitrate in fine particles is usually under significantly neutralized or ammonium-rich conditions (Pathak et al., 2009). There are various factors influencing the formation of aerosol sulfate and nitrate, such as the levels of

gaseous precursors (SO_2, NH_3, NO_X) and oxidants, the characteristics of pre-existing aerosols, and meteorological conditions. These factors may vary by location, resulting in different formation mechanism in different areas. For instance, different formation pathways had been reported for nitrate in ammonia-rich and ammonia-deficient areas (Pathak et al., 2009).

In January 2013, extremely severe, persistent and widespread haze weather occurred in 10 provinces in central and eastern China. These serious pollution events not only had great adverse effects on human health, as seen in a sharp increase in respiratory diseases, but also caused immeasurable economic loss (Huang et al., 2014; Chen et al., 2013). High secondary inorganic and organic aerosol contributions to particulate pollution during these haze events were reported in a recent study based on the measurements at urban sites in Beijing, Shanghai, Guangzhou and Xi'an, which located in the northern, eastern, southern and western regions of China, respectively (Huang et al., 2014). In addition to investigating primary particulate emissions, the formation mechanisms of these secondary species and related affecting factors also need to be understood in order to controlling $PM_{2.5}$ levels in China.

The Yangtze River Delta (YRD), the Pearl River Delta, Beijing–Tianjin–Tangshan, and the Sichuan Basin are the four regions with heaviest haze influence in China. The characteristics and formation mechanisms of haze in the YRD are different from other haze regions, such as Beijing and the Pearl River Delta (Fu et al., 2008). Suzhou is located in the heartland of YRD region and is an important city. It suffered from the extremely serious aerosol pollution in Jan. 2013. With the tremendous economic growth over the past 30 years, Suzhou has experienced high levels of air pollution as reflected in the frequency of haze occurrence. The annual haze days in Suzhou increased from only two days to more than 150 days from 1956 to 2011, i.e. over 40% of days were hazy in 2011. The low visibility, particularly the haze, has become a major concern of the city. However, only a few studies have focused on haze events in Suzhou and little is known about the chemical characteristics and sources of fine particles in this city. To fill these knowledge gaps,

an intensified monitoring campaign was launched from December 2012 to January 2013 to collect high temporal resolution chemical and meteorological data. The objectives of this study are to (1) identify the dominant species in $PM_{2.5}$ and responsible for the visibility reduction; (2) explore the formation mechanism of the aerosol pollution; (3) study the impact of local, nearby and remote sources on the formation of haze in urban Suzhou.

2. Methodology

2.1 Field observations

The sampling station was set up at the roof of one building in Suzhou Institute of Environmental Sciences (31°20'N, 120°36'E) (Fig. 1), about 300 m west to Nanyuan South Road and 360 m north to S Ring Road Elevated Bridge. There is no industrial source nearby and the site is representative of an urban residential and commercial environment. Suzhou is located in the center of Yangtze River Delta (YRD) and about 80 km east of Shanghai and 200 km west of Nanjing.

On-line hourly $PM_{2.5}$ mass concentrations were measured using tapered element oscillating microbalance (TEOM1405, Thermo Scientific Corp., MA, US) with the heating temperature of 50 ºC. Some of the volatile particulate matter might be lost at 50 ºC, but comparisons with collocated filters showed that the loss was less than 10%-20% of the gravimetric mass (Chow et al., 2008).

Hourly real-time concentrations of five cations (Na^+, K^+, NH_4^+, Ca^{2+}, and Mg^{2+}) and four anions (F^-, Cl^-, NO_3^-, and SO_4^{2-}) in $PM_{2.5}$ were determined by URG Series 9000 Ambient Ion Monitor (AIM, URG Corporation, Chapel Hill, NC). The system consists of a particle collection unit and two ion chromatograph analyzers for cation and anion analyses. $PM_{2.5}$ was separated by a sharp-cut cyclone inlet operating at a flow rate of 3 L/min. The air was drawn through a liquid diffusion parallel-plate denuder to remove the interfering acidic and basic gases. A Steam-Jet Aerosol

Collector was placed downstream of the denuder for collection and extraction of particles. The water extract was subsequently injected into the two ICs once an hour. The estimated uncertainties of the AIM measurements were approximately less than 15% (Trebs et al., 2004; Pathak et al., 2011). Some measures were taken out to reduce error, for instance, standards solutions were periodically injected to check the consistency of sensitivity of the detectors and air flow rate is frequently checked using a calibrated flow meter.

A semi-continuous OC/EC analyzer (Sunset Laboratory, Forest Grove, Oregon, USA) was applied to determine the carbonaceous species in $PM_{2.5}$. This instrument used the thermal-optical transmittance method based on NIOSH Method 5040. Organic compounds were vaporized in pure helium and then oxidized to CO_2 in a manganese dioxide oxidizing oven. CO_2 was then quantified by non-dispersive infrared detector. EC was then desorbed in an oxygen blend carrier gas and then oxidized and quantified using the same method as for OC. The split point between the pyrolized carbon formed from the organic carbon during the heating and EC that was originally in the sample was determined by measuring the transmission of a laser beam through the filter. Known volume of methane was injected, oxidized and quantified as an internal standard. Good correlations were found between the data measured by this instrument and filter-based laboratory analyses (Bae et al., 2004).

Visibility was monitored using the Belfort Model 6000 Visibility Sensor (Belfort Instrument Corp., MD, US). Trace O_3, SO_2, NO-NO_2-NO_X and CO gases were obtained with a resolution of 1 h by applying online analyzers (Thermo Instruments, TEI 49i, 43i, 42i and 48i, respectively). Meteorological parameters were collected using Met Station One (Met One Corp., OR, US).

2.2 Data analysis methods

2.2.1 Reconstruction of the light extinction coefficient

The light extinction (b_{ext}) which is the sum of light scattering by particle ($b_{s,p}$), absorption by particle ($b_{a,p}$), scattering by gas ($b_{s,g}$), and absorption by gas ($b_{a,g}$), is reconstructed according to the revised IMPROVE algorithm as following (Pitchford et al., 2007):

$$b_{ext} = b_{s,p} + b_{a,p} + b_{a,g} + b_{s,g}$$

$$\approx 2.2 \times f_S(RH) \times [\text{Small } (NH_4)_2SO_4] + 4.8 \times f_L(RH) \times [\text{Large } (NH_4)_2SO_4]$$

$$+ 2.4 \times f_S(RH) \times [\text{Small } NH_4NO_3] + 5.1 \times f_L(RH) \times [\text{Large } NH_4NO_3]$$

$$+ 2.8 \times [\text{Small OM}] + 6.1 \times [\text{Large OM}]$$

$$+ 1 \times [\text{Fine Soil}] + 1.7 \times f_{SS}(RH) \times [\text{Sea Salt}]$$

$$+ 0.6 \times [\text{Coarse Mass}] + 10 \times [\text{EC Mass}]$$

$$+ 0.33 \times [NO_2 \text{ (ppb)}] + \text{Rayleigh Scattering} \quad (1)$$

where $f_S(RH)$ and $f_L(RH)$ are the water growth factors for small- and large-sized distribution of sulfate and nitrate, respectively, and $f_{SS}(RH)$ is the water growth factor for sea salt. Water growth factors are adopted according to Pitchford et al. (Pitchford et al., 2007). The constant numbers in the above equation are extinction efficiencies for each chemical species under dry condition. $(NH_4)_2SO_4$ mass is estimated as 1.38 times of SO_4^{2-} mass and NH_4NO_3 mass 1.29 times of NO_3^- mass assuming that SO_4^{2-} and NO_3^- are fully neutralized by NH_4^+ in the forms of $(NH_4)_2SO_4$ and NH_4NO_3, respectively, according to the revised IMPROVE method. Organic matter (OM) is estimated as 1.8 times of OC concentration to account for unmeasured fractions.

The concentrations of sulfate, nitrate, and OM are divided into small- and large-sized fractions in this algorithm. The size modes are described by log-normal mass size distributions with geometric mean diameter and geometric standard deviations. Concentrations of sulfate, nitrate, and OM in the large- and small-mode are estimated using the following equations (taking sulfate as an example):

$$[\text{Large } (NH_4)_2SO_4] = [\text{Total } (NH_4)_2SO_4]^2/20, \text{ for } [\text{Total } (NH_4)_2SO_4] < 20\ \mu g\ m^{-3} \quad (2)$$

$$[\text{Large } (NH_4)_2SO_4] = [\text{Total } (NH_4)_2SO_4], \text{ for } [\text{Total } (NH_4)_2SO_4] > 20\ \mu g\ m^{-3} \quad (3)$$

184 [Small $(NH_4)_2SO_4$] = [Total $(NH_4)_2SO_4$] - [Large $(NH_4)_2SO_4$] (4)

185

186 **2.2.2 Air mass back trajectory**

187 To study the impact of local and regional sources on the aerosol pollution in Suzhou,
188 48-h back trajectories starting at 100 m from the sampling site were calculated using
189 the NOAA HYSPLIT model (http://ready.arl.noaa.gov/HYSPLIT_traj.php). The back
190 trajectories were calculated four times per day at starting times of 04:00, 10:00, 16:00,
191 and 22:00 UTC, i.e. 12:00, 18:00, 00:00, and 06:00 local times, respectively. The
192 trajectory cluster analysis was based on the GIS-based software TrajStat (Wang et al.,
193 2009).

194

195 **2.2.3 Potential source contribution function**

196 The potential source contribution function (PSCF) method is based on the results of
197 HYSPLIT model and can be used to identify the regional sources. The zone of
198 concern is divided into $i \times j$ small equal grid cells. The PSCF value for the ijth grid
199 cell is calculated as: $PSCF_{ij} = m_{ij}/n_{ij}$, where n_{ij} is designated as the number of
200 trajectory segment endpoints that fall in the ijth cell and m_{ij} is defined as the number
201 of trajectory endpoints with pollutants concentrations higher than an set criterion
202 (Ashbaugh et al., 1985; Wang et al., 2009). In present study, the average
203 concentrations were treated as the criterion (Hsu et al., 2003). The PSCF values were
204 multiplied by a weighting function W_{ij} to reduce the effect of small values of n_{ij} and to
205 better reflect the uncertainty in the values for the cells with small n_{ij} values. The
206 weighting function W_{ij} is defined as follows (Polissar et al., 1999):

207
$$W_{ij} = \begin{cases} 1.00, & 80 < n_{ij} \\ 0.70, & 20 < n_{ij} \le 80 \\ 0.42, & 10 < n_{ij} \le 20 \\ 0.05, & n_{ij} \le 10 \end{cases}$$

208

The PSCF value can be interpreted as the conditional probability that air masses with pollutants concentration greater than the set criterion pass through the *ij*th cell during transport to the receptor site (Wang et al., 2009). That is, cells with high PSCF values are indicative of regions having high potential contributions to the pollution at the receptor site.

3. Results and discussion

3.1 General characteristics of haze events

As illustrated in Fig. 2, the visibility varied from a few hundred meters to more than 50 km with a minimum value of only 322 m on Jan. 15, 2013, which was accompanied by high RH (82%). During the 2-month observation period, there were a total of ten periods when visibility was below 10 km. Excluding the five periods accompanied by precipitation, the other five periods were identified as haze events and all of these events occurred in January 2013. During the haze occurrence, hourly concentrations of $PM_{2.5}$ often exceeded 150 μg m^{-3}, with a maximum concentration of 324 μg m^{-3} observed on Jan. 14, 2013. These concentrations were generally higher than those in normal periods. The daily concentrations of $PM_{2.5}$ on haze days varied from 148 to 196 μg m^{-3}, which were 1.97 to 2.61 times the Grade II criteria of the national ambient air quality standard (75 μg m^{-3}). These values were comparable to that observed in Nanjing where the average $PM_{2.5}$ was 175.6 μg m^{-3}, but slightly higher than those in some other cities in YRD where mean values were generally lower than 147.3 μg m^{-3} when haze occurred in Jan. 2013 (Wang et al., 2014a; Wang et al., 2014d). The aerosol pollution happened in northeast China such as in Beijing, Tianjin, and Shijiazhuang were much severer, for instance, the daily and hourly concentrations of $PM_{2.5}$ were up to 368 μg m^{-3} and 462 μg m^{-3} in Tianjin in January 9 to 13, 2013, and the maximum hourly value of approximately 1000 μg m^{-3} was recorded in Beijing and Shijiazhuang in Jan. 2013 (Ji et al., 2014; Han et al., 2014; Wang et al., 2015).

Approximately 40% of the time in January 2013 met haze weather criteria, whereas no haze appeared in December 2012. Low amount of rainfall in January might be one of the factors causing the long duration of haze. Relative humidity (RH) was reported to be an important contributor to the visibility reduction. In the present study, visibility decreased with increasing RH, e.g. when RH increased from 42% to 78%, visibility decreased from 42 km at 2:00 p.m. on 17 January to 4 km at 7:00 a.m. on 19 January. Statistically, RH was relatively higher during haze occurrence than clear periods. Low wind speed, smaller than 5 m s^{-1}, was frequently observed during this winter. Furthermore, wind speed was mostly less than 1 m s^{-1} during the haze events, lower than those in Beijing (Yang et al., 2015). Besides, atmospheric pressure was also found to be relatively low during the haze occurrences. The stagnant air, due to low wind speed and pressure, was unfavorable for aerosol horizontal transport or vertical diffusion, and therefore resulted in aerosol accumulation. Therefore, unfavorable weather conditions (high RH, and low rainfall, wind speed and atmospheric pressure) were among the causes forming haze in January 2013 in Suzhou as well as in many other cities (Wang et al., 2014b; Wang et al., 2014c; Wang et al., 2014d; Han et al., 2014; Yang et al., 2015).

In order to get more insights of the haze formation in this region, three haze events, which occurred on Jan. 19, from Jan. 21 to 26, and on Jan. 30, respectively, were further discussed below. Generally, the meteorological parameters and aerosol pollution level were comparable during these three haze occurrences, except for the relatively lower RH and higher temperature in the third haze events.

3.2 $PM_{2.5}$ chemical composition and light extinction

3.2.1 $PM_{2.5}$ chemical composition

The temporal variations of the concentrations of water-soluble inorganic ions (WSIIs) are illustrated in Fig. 3. The mean concentration of WSIIs (including four anions and

five cations) was 48.8 ± 24.6 μg m^{-3}, accounting for 40% of $PM_{2.5}$ mass concentration, slightly lower than that in Beijing which was 69.4 ± 55.8 μg m^{-3} and accounted for 43% of $PM_{2.5}$ (Tao et al., 2015). SO_4^{2-} was the most abundant species in WSIIs, with averaged value of 21.1 ± 13.5 μg m^{-3}, followed by NH_4^+ (13.9 ± 5.69 μg m^{-3}) and NO_3^- (10.7 ± 6.75 μg m^{-3}), accounting for 43%, 29% and 21% of WSIIs, respectively. These secondary inorganic components in total constitute 93% of total WSIIs, close to the result in Beijing (Gao et al., 2015; Tao et al., 2015). The rest of ions, Na^+ (1.36 ± 0.43 μg m^{-3}), K^+ (0.85 ± 0.45 μg m^{-3}), Cl^- (0.54 ± 1.28 μg m^{-3}), Ca^{2+} (0.34 ± 0.27 μg m^{-3}), F^- (0.06 ± 0.72 μg m^{-3}), Mg^{2+} (0.05 ± 0.07 μg m^{-3}), each had minor contribution (< 3%) to WSIIs.

NO_3^- and SO_4^{2-} are mainly formed from the transformation of their respective gaseous precursor of NO_X and SO_2 (Wang et al., 2005). The emission ratio of NO_X to SO_2 was 17.2–52.6 for motor vehicles and 0.527–0.804 for stationary sources in the Yangtze River Delta, which means that the emissions of SO_2 from motor vehicles were much less than NO_X, but the emissions of SO_2 from stationary sources such as power plants, industrial boilers and furnaces were relatively higher than NO_X (Fu et al., 2008). Thus, the mass ratio of NO_3^-/SO_4^{2-} could be used as an indicator of the relative importance of mobile and stationary sources of sulfur and nitrogen in the atmosphere (Arimoto et al., 1996). In the present study, the averaged ratios of NO_3^-/SO_4^{2-} and NO_X/SO_2 were 0.59 and 5.68, respectively, indicating that emissions from vehicles and stationary sources were both important in Suzhou. The ratio of NO_3^-/SO_4^{2-} in this study was lower than that in Beijing, but higher than those in Shanghai (0.43), Qingdao (0.35), Taiwan (0.20), and Guiyang (0.13) (Wang et al., 2006; Yao et al., 2002; Hu et al., 2002a; Fang et al., 2002; Xiao and Liu, 2004).

The NO_3^-/SO_4^{2-} ratio was relatively higher for 20% worst visibility hours (0.58) than 20% best visibility hours (0.54), suggesting that vehicle emission might play an important role in haze pollution. This was in agreement with the result in Guangzhou, where the NO_3^-/SO_4^{2-} ratio was 1.02 under stagnation and 0.55 in normal days, but contrary to that in Beijing, where the ratio in haze days (0.89) was lower than in

normal days (0.96) (Tan et al., 2009; Wang et al., 2006). In present study, NO_X concentration greatly exceeded that of SO_2 during haze period, coincided with the result in Guangzhou, but disagreed with that in Beijing (Tan et al., 2009). Previous studies have indicated that high NO_X emission may reduce the formation of OH and H_2O_2, and further decrease the possibility of SO_4^{2-} formation (Tan et al., 2009). Thus, the elevation of NO_3^- concentration under worse visibility conditions was greater than that of SO_4^{2-} in both Suzhou and Guangzhou. The ratios of (NO_3^-/SO_4^{2-}) to (NO_X/SO_2) were lower for worse visibility period, in accordance with that in Beijing, showing that the nitrate concentrations may be also greatly affected by the re-volatilization of NH_4NO_3 (Tan et al., 2009).

The carbonaceous species, constituting 22% of $PM_{2.5}$, were dominated by organic carbon, which was 22.8 ± 10.6 μg m^{-3} and 3 to 29 times of that of elemental carbon (2.79 ± 2.58 μg m^{-3}), similar to those in Beijing (Tao et al., 2015). The relatively high ratios of OC/EC (10.6 ± 4.29), which were higher than the ratios in Beijing (7.1 ± 0.5) and Jinan (7.15 ± 1.78), demonstrated the existence of secondary organic carbon (SOC) (Ji et al., 2014; Zhang et al., 2014). The concentrations of SOC were estimated by applying the EC tracer method, which has been widely used to estimate the secondary organic aerosol contribution to $PM_{2.5}$ concentrations (Castro et al., 1999; Yang et al., 2005). The minimum ratio of OC/EC was 3.09 in the present study. The estimated SOC was 14.2 ± 5.69 μg m^{-3}, contributing 65% on average to OC. The SOC/OC was higher than 0.5 during almost the whole sampling period except on Jan. 30 when the third haze event occurred. This ratio was higher than most of the results found in other areas such as in Beijing and Guangzhou (Yang et al., 2005; Tan et al., 2009).

Major components in $PM_{2.5}$ were found to be SO_4^{2-} (17%), SOC (14%), NH_4^+ (12%), NO_3^- (8%), and POC (6%). The top four components were mainly from secondary sources. $PM_{2.5}$ was significantly correlated with these secondary species, revealing that gas to particle conversion was severe in winter and had great impact on aerosol pollution in this region. It's worth noting that the aerosol composition in the

third haze event was distinct from the other two (Fig. 3) as seen from the higher proportion of carbon species from primary emissions (POC and EC) and lower fraction of secondary formation components (SIA and SOC), indicating different haze formation mechanism in the third haze event.

3.2.2 Light extinction coefficient

In order to determine the contribution of $PM_{2.5}$ constituents to the visibility degradation, light extinction (b_{ext}) was reconstructed based on the revised IMPROVE algorithm. In the present study, the impact of fine soil and coarse mass were not included because of the lack of metal elements and coarse matter concentrations. The estimated b_{ext} was 664 ± 288 Mm^{-1} and was significantly correlated with $PM_{2.5}$ concentrations (r = 0.94, p < 0.001), demonstrating the strong influence of fine aerosols on visibility degradation.

The reconstructed light extinction coefficient was compared with that derived from visibility and that calculated using a regression model developed by Chen. Extinction coefficient is inversely correlated with visibility according to the Koschmieder equation (Vis = K/b_{ext}) (Seinfeld and Pandis, 2012). By using a K value of 3.912, the calculated b_{ext} was 371 ± 234 Mm^{-1}, much lower than the coefficients obtained from IMPROVE algorithm. Nevertheless, they were significantly correlated with each other (r = 0.71, p < 0.001). Another method applied here to estimate b_{ext} was a 2-factor parameterization regression model based on RH and aerosol volume concentration (Chen et al., 2012). The volume concentration can be acquired from the mass concentration divided by an average particle density of 1.7 g cm^{-1} (Wehner et al., 2008). A comparison of b_{ext} reconstructed by IMPROVE algorithm and the regression model is presented in Fig. 4. Generally, a strong correlation was evident with a correlation coefficient higher than 0.97 (R^2 = 0.952), confirming that the reconstructed b_{ext} from the IMPROVE algorithm was reliable. The majority of b_{ext} was clustered near the 1:1 line for b_{ext} < 500 Mm^{-1}, with the corresponding RH mainly below 75%.

However, for b_{ext} > 500 Mm^{-1}, the dispersion of b_{ext} gradually increased, and most of the corresponding RH was higher than 75%. There are two possibilities causing these deviations. The first one is the ignorance of the impact of particle size distribution on light extinction in the 2-factor parameterization model applied here, as the variation of aerosol mass or volume fractions of different size particles can influence b_{ext} value especially under high RH (Chen et al., 2012). The second one is from the uncertainties of in situ measurements since RH sensor may have large errors under high RH condition. The regression model result was directly controlled by the RH value, and the hygroscopic growth factor in the IMPROVE algorithm depends on RH.

The light extinction was mostly influenced by aerosol light scattering as the estimated $b_{s,p}$ was 609 ± 277 Mm^{-1}, accounting for 91% of b_{ext}, while $b_{a,p}$ and the extinction coefficient by gaseous were only 27.9 ± 25.8 Mm^{-1} and 26.6 ± 4.87 Mm^{-1}, respectively. The largest contributor to b_{ext} from the reconstructed chemical species in fine particles was organic matter (OM), accounting for 40%, followed by $(NH_4)_2SO_4$, 34%, NH_4NO_3, 16%, and EC, 4%. However, the percentage contributor varied greatly during the study period, e.g. the contributions of NH_4NO_3 ranged from only 3% to up to 40%. Generally, the contributions of $(NH_4)_2SO_4$ and NH_4NO_3 were higher under low visibility period, increased from 30% and 11%, respectively, during the 20% best visibility periods to 39% and 19%, respectively, during the 20% worst visibility period. Correspondingly, the contributions of OM and EC reduced from 46% and 5%, respectively, to 35% and 4%, respectively, during the same periods. These results indicated the important role sulfate and nitrate played on haze formation.

The percentage contribution to light extinction from individual aerosol components also varied with haze event and visibility conditions. The percentage contributions of individual components during the best and worst 20% visibility hours in each of the three haze events are compared and shown in Fig. 5. During the first haze event (on Jan. 19), the contribution of NH_4NO_3 was 8% and 24% during the 20% best and worst visibility hours, respectively, while the corresponding numbers are 48% and 37% for OM. There were no significant differences between the two

visibility categories for the contributions of $(NH_4)_2SO_4$ or EC. During the second haze event (from Jan. 21 to 26), the fractions were 1.8, 1.5 and 1.3 times higher for NH_4NO_3, $(NH_4)_2SO_4$ and EC respectively but 1.2 times lower for OM under 20% worst visibility condition than those under 20% best visibility condition during this time. Overall, $(NH_4)_2SO_4$ made great contribution to the light extinction and NH_4NO_3 had largest difference between 20% best and worst visibility conditions during these two haze events. Therefore, secondary inorganic aerosols especially NH_4NO_3 was likely the key component for the impaired visibility for these two haze events. The elevated proportion of $(NH_4)_2SO_4$ and NH_4NO_3 during the heavy polluted period was also observed in Beijing (Tao et al., 2015; Wang et al., 2015; Zheng et al., 2015). A different trend of comparison between the best and worst visibility periods was found in the third haze event (on Jan. 30) than in the first two. In the third event, the percentage contributions of OM and EC increased during the worst visibility period compared to the best visibility period (from 40% to 49% and 6.8% to 11%, respectively), while that of $(NH_4)_2SO_4$ decreased (from 28% to 19%). Carbonaceous components played a more important role for visibility reduction in the third event. Therefore, there seems to be different formation mechanisms for haze events in Suzhou.

3.3 Conversion from gas to particle phase

3.3.1 Variations of aerosol particles and precursors

Fig. 6 diagrammed the diurnal variations of meteorological parameters, various aerosol components, gaseous precursors, and some other important gaseous species under three different visibility conditions: (1) all data, (2) visibility ≤ 10 km, and (3) visibility > 10 km. The daily variations of gas-phase compounds were different between species and were mainly controlled by the direct surface emissions (such as NO_X, SO_2, and CO) or photochemical process (O_3). There were a distinct morning peak and a less distinct afternoon peak, consistent with morning and afternoon rush

hours for NO_X and CO. This might be related to the heavy traffic emissions in the rush hours and the strong elevation of the Planetary Boundary Layer heights at noon. In contrast, there was only one mid-day peak for SO_2. This diurnal profiles were similar to those observed in Guangzhou (Hu et al., 2002b) and Maryland (Antony Chen et al., 2001). In the latter study, the dominant source of SO_2 was considered to be the long range transport from the industrialized Midwest and with the deep boundary layer around noon; SO_2 aloft mixed more effectively down to the surface and thus caused the mid-day peak of SO_2. The reasons for the diurnal variation of SO_2 observed in the present study need further investigation. Similar to the diurnal distribution of SO_2, O_3 also showed one distinct peak around noon due to the strong photochemistry at that time (Quan et al., 2014).

For the aerosol components, EC which was also produced by the surface emissions showed a profile similar to NO_X and CO. Furthermore, EC had significantly positive correlation with NO_X and CO, demonstrating that they had common sources, mainly from vehicular exhaust. The diurnal profiles of the secondary species were similar to their precursors but obviously affected by other factors such as solar radiation, which could promote the oxidation of the precursors. For instance, there was a 2-hour delay for sulfate to reach its peak compared to SO_2 due to the transformation processes. This pattern was also observed in Guangzhou (Hu et al., 2002b). NO_3^- and SOC exhibited similar diurnal variation as their precursors had common sources and they both formed from secondary photochemical oxidation. The daily profiles of NO_3^-, NH_4^+ and SOC showed lower concentrations around 15:00 (local time) probably due to the high boundary layer and/or low concentration of precursors. Besides, for NO_3^- and NH_4^+, high temperature, which enhanced the evaporative loss, and low relative humidity may also be responsible for the low levels.

Fig. 6 also suggested that both gas-phase compounds and aerosol components all showed similar patterns of diurnal variations but had different magnitudes of concentrations for different visibility levels. These components except for O_3 all

showed relatively higher concentrations under low visibility especially for the secondary inorganic species, indicating the important impact of the formation of secondary components on the visibility reduction. The relatively low levels of O_3 under low visible conditions might be due to the decreased photochemical production and the chemical conversions of SO_2 and NO_X to sulfate and nitrate. It is worth noting that the relatively high humidity which favored the formation of sulfate and nitrate was observed under low visibility conditions. In addition, it seemed that low visibility was associated with southwest wind. This might related to the topography. There are mountains located on the southwest which is not conducive to the diffusion of pollutants.

In consideration of the distinct aerosol composition during the third haze, the comparison of gaseous pollutants between the third and the first two haze episodes were made. The concentrations of SO_2 and O_3 were comparable for these three haze event. Contrarily, much higher levels of NO, CO and NO_2 were evident during the third haze, in accordance with the high concentrations of POC and EC. These species (NO, CO, NO_2, POC and EC) had good correlations with each other. Furthermore, they had similar diurnal variations and exhibited extremely high levels in the morning rush hours on January 30 when the third haze occurred. These results implied that there were common sources for these species, mainly from vehicle exhaust emission.

3.3.2 Formation mechanisms of sulfate and nitrate

As discussed earlier, the chemical formation of sulfate and nitrate from SO_2 and NO_2 respectively, should play important roles for visibility reduction, especially for the first two haze events. The sulfur oxidation ratio, defined as SOR = $n\text{-}SO_4^{2-}/(n\text{-}SO_4^{2-} + n\text{-}SO_2)$ and the nitrogen oxidation ratio, defined as NOR = $n\text{-}NO_3^-/(n\text{-}NO_3^- + n\text{-}NO_2)$ were used as indicators of the secondary transformation processes. The daily variations of NOR showed similar patterns as those of NH_4^+ and NO_3^-. Likewise, SOR had similar diurnal changes as SO_4^{2-}. The values of SOR and NOR increased

more than 1.3 and 2.0 times, respectively, during the first two haze periods compared to clear periods, implying greater oxidation of gaseous species and more elevated secondary aerosols. This was supported by the evidently higher concentrations of SO_4^{2-}, NH_4^+, and NO_3^- in the first two haze events. Almost no elevating levels of SOR, NOR or SIA were observed in the third haze, again confirming that the SIA formation may not be the predominant factor controlling the occurrence of this haze event.

The formation of SO_4^{2-} from SO_2 was mainly ascribed to the gas-phase oxidation by OH and H_2O_2 radical or heterogeneous oxidation (Wang et al., 2006; Zhao et al., 2013). The gas-phase reaction is a strong function of temperature and heterogeneous reactions always associated with high RH (Sun et al., 2006; Sun et al., 2014; Sun et al., 2013a). However, weak correlations were found between SOR and either temperature ($r = 0.174$, $p < 0.01$) or RH ($r = 0.150$, $p < 0.01$) in the present study, indicating the complex formation mechanism of sulfate.

Many studies suggested that sulfate from aqueous SO_2 oxidation catalyzed by transition metals was more significant during winter haze rather than gas-phase oxidation (Li et al., 2011; Sun et al., 2013b; Zhao et al., 2013). Our measurement also found that the heterogeneous oxidation was an important sulfate formation pathway in this study area. As shown in Fig. 7, high concentrations of NO_2 accompanied with ultralow level of O_3 less than 10 ppb and low amount of solar radiation were observed during most of the time in the haze period, such as from 12 PM to 10 AM on 19 January and from 21 to 34 January. These results revealed the rather weak photochemical activities during these time windows. The high levels of NO_2 and weak photochemical activities could result in insufficient production of oxidants (OH and H_2O_2 radicals) for gas-phase oxidation (Hua et al., 2008). Thus, other oxidation reactions other than gas-phase oxidation likely explained the formation of abundant secondary sulfates during the haze episode. The high RH (> 70%) during these haze period was a beneficial factor for aqueous-phase oxidation of SO_2 to sulfate. Besides, the calculation results using the Extended AIM Aerosol Thermodynamic Model (E-AIM, Model II) (Clegg et al., 1998) (http://www.aim.env.uea.ac.uk/aim/aim.php)

showed a significant increase of the liquid water content when RH > 70%. These results highlight the importance of aqueous-phase reaction to the secondary transformation of SO_2.

The concentrations of O_3 were not extremely low during the whole haze period, such as during daytime on January 23 and 25; the O_3 levels were as usual and had obvious diurnal variations with one distinct peak around noon. RH was lower than 70% and sulfate was primarily in the solid phase at these times, indicating that gas-phase oxidation was probably the dominant pathway for sulfate formation. Aqueous-phase oxidation likely became predominant at night. This could explain the high SOR in the afternoon and the sustained high level at night.

Nitrate formation is mainly through gas-phase oxidation of NO_2 by OH during daylight and the heterogeneous reactions of nitrate radical during nighttime (Seinfeld and Pandis, 2012). Fig. 8 showed the nitrate-to-sulfate molar ratio ($[NO_3^-]/[SO_4^{2-}]$) as a function of the ammonium-to-sulfate molar ratio ($[NH_4^+]/[SO_4^{2-}]$), which can provide an insight into the formation pathway of the secondary species (Jansen et al., 2014; Pathak et al., 2009; He et al., 2012). The relative abundance of nitrate linearly increased with the increasing ammonium-to-sulfate molar ratio. Fitting a linear regression line resulted in an intercept of $[NH_4^+]/[SO_4^{2-}]$-axis of 1.51, indicating that nitrate formation via homogeneous reaction of HNO_3 with NH_3 became significant at $[NH_4^+]/[SO_4^{2-}] > 1.51$ (Pathak et al., 2009; Jansen et al., 2014; He et al., 2012). Pathak et al. (2009) also reported an intercept value of 1.5 for several cities worldwide while Jansen et al. (2014) found a slightly smaller intercept value of 1.38 for Hangzhou. The ammonium concentration in excess of the amount at which nitrate formation became evident was defined as excess ammonium ($[NH_4^+]_{exc} = ([NH_4^+]/[SO_4^{2-}]-1.51)\times[SO_4^{2-}]$). The concentrations of excess ammonium were always higher than 0 and linearly correlated with nitrate concentration, as shown in Fig. 8. This indicated that the formation of nitrate was strongly associated with ammonium formation. In other words, when the excess ammonium was > 0, the gas-phase homogeneous reaction between the ambient ammonia and nitric acid was responsible for forming nitrate

(Pathak et al., 2009; Jansen et al., 2014). The slope of 0.37 for the regression and the scattering of the data indicated that the excess ammonium was bound to species other than nitrate, such as chloride, bisulfate, etc. The significance of gas-phase homogeneous reaction to nitrate formation has been reported for many cities (Jansen et al., 2014; Pathak et al., 2009). However, as mentioned above, in some cases during haze period, the conditions (ultralow ozone concentrations, low solar radiation and high NO_2) were not favorable for the gas-phase oxidation. Relatively high RH were often observed in those cases, which may have favored the gas to particle partitioning of nitrate acid and ammonia (Sun et al., 2011). Furthermore, the E-AIM calculation results manifested that the nitrate partly or completely existed in the aqueous phase during those conditions. Therefore, we assumed that heterogeneous chemistry, such as heterogeneous hydrolysis of N_2O_5 ($N_2O_5 + H_2O$ (aq) $\rightarrow 2HNO_3$) or equilibrium partitioning (HNO_3 (g) + NH_3 (g) $\leftrightarrow$ NH_4^+ (aq) + NO_3^- (aq)) also contributed to the formation of nitrate under high RH conditions. This was supported by the fact that in Fig. 8 more plots were deviated from the regression line when RH were relatively high. The importance of heterogeneous reactions for nitrate formation were also reported in other studies (Sun et al., 2011; Zheng et al., 2015).

3.4 Regional sources deduced from trajectory and PSCF analyses

The regional sources and transport of air pollutants exert a profound impact on local air quality in YRD region as it is located in the typical monsoon region (Ding et al., 2013). Therefore, trajectory clustering method was employed to examine the pathway of air masses and to look into the chemical composition and light extinction coefficients among the air masses with different origination. The calculated 48-h back trajectories were clustered into six clusters (Fig. 9 and Table 1), i.e. six air mass transport pathways. As can be seen, air masses reaching at Suzhou mainly came from local areas, the nearby provinces (cluster 2, accounting 31.7%), and the northwestern areas (cluster 1 and 3, both accounted for 20.6%).

High aerosol concentrations were associated with these trajectories. This was reasonable considering that these air masses passed over some highly industrialized cities, such as Hefei, Nanjing, and Hangzhou (Fig. 1). Relatively low levels of $PM_{2.5}$ were related to clusters 5 and 6. Based on the pathways and origins, these air masses were expected to bring in relatively clean air from the East China Sea and the Yellow Sea and consequently reduced the aerosol pollution in Suzhou.

Aerosols had high fractions of secondary inorganic ions (39%-42%) and relatively low contributions of OC (15%-16%) when the air masses fell in the C1, C3 and C4, while had relatively high percentage of OC (36%) when the air masses fell into the C5. These differences of aerosol concentrations and composition in different clusters may result in distinct light extinction coefficients and species contributions to visibility reduction when air masses originated from different directions (Fig. 9). Similar to $PM_{2.5}$, the reconstructed b_{ext} was the highest when air masses originated from the Northwest area (C3) and was relatively low when air masses fell into C5 and C6 areas. However, the lowest value of b_{ext} was in the C6 instead of C5 for the lowest $PM_{2.5}$ level, because of the higher contribution of OM in the C5. AS and OM were the dominant species determining the light extinction for all clusters. However, AS was the predominant contributor to light extinction for trajectories from north and northwest (C1, C3, C4), while in other cases the light extinction was primarily affected by OM. AN was the third highest contributor in all trajectory clusters with the largest contribution when air masses originated from northwest.

The origins of air masses in different haze events were further analyzed to interpret the relative contributions of chemical species to visibility reduction that differed between haze events. Most air masses fell into C1 and C3 (air masses from north and northwest, respectively) in the first two haze occurrence while all air mass trajectories were in C2 (air masses from local and nearby areas) for the third haze event. The contribution of OM to the total light extinction was higher in the third haze event than in the first two as discussed early, consistent with the results for cluster analysis that the light extinction was primarily impacted by AS for C1 and C3 but by

OM for C2. These results manifested that the third haze event was mainly contributed by the primary emission of carbon species from the local and/or surrounding areas.

It should be noted that air mass back trajectory analysis only suggests the originations and pathways of air masses but does not directly reveal the exact sources. Based on the results of trajectory analysis, the PSCF method was applied to explore the likely regional sources of major components in $PM_{2.5}$, including sulfate, nitrate, OC, and EC, as illustrated in Fig. 10. Generally, $PM_{2.5}$ and the five aerosol species in Suzhou were mainly affected by local sources and nearby cities. Specifically, the higher value for $PM_{2.5}$ and the aerosol components were all localized in northwest to the south, covering surrounding cities in Jiangsu and near the border of Anhui and Zhejiang provinces. Additionally, these species were all affected by pollutions from Anhui province. Sulfate, nitrate and ammonium had similar spatial distributions, and relatively more affected by the north and northwest cities in Shandong, Jiangsu and Anhui provinces while pollutions from south cities in Zhejiang province had more impact on OC and EC in studied area than sulfate, nitrate and ammonium.

4. Conclusions

Heavy aerosol pollution occurred in Suzhou in January 2013 with daily $PM_{2.5}$ concentrations on haze days 1.97 to 2.61 times higher than Grade II criteria of the national ambient air quality standard (75 μg m^{-3}) and maximum value of 324 μg m^{-3} on Jan. 14, 2013. Unfavorable weather conditions (high RH, low rainfall, wind speed and atmospheric pressure) especially high RH together with increased air pollutants produced from local and nearly sources were responsible for these haze formation.

During the first two haze periods, the major aerosol components were SO_4^{2-}, NO_3^-, NH_4^+, and SOC, which were mainly from secondary sources. Furthermore, SOR and NOR both increased under worst visibility conditions, revealing efficient gas to particle conversion. Additionally, the contributions of $(NH_4)_2SO_4$ and NH_4NO_3 to the reconstructed b_{ext} based on IMPROVE were higher under low visibility

conditions while those of OM and EC were higher under high visibility conditions, indicating that secondary inorganic aerosols especially NH_4NO_3 seemed to be very important for the impaired visibility. Gas-phase homogeneous reaction might dominate the formation of sulfate and nitrate under low RH conditions while heterogeneous process might be responsible when RH were relatively high.

Distinctively, high proportion of carbon species from primary emission and lower fraction of secondary formation components were observed in the third haze. The SOR and NOR during the third haze episode were comparable to clean days. Moreover, increasing proportions of OM and EC accompanied with decreasing percentage of $(NH_4)_2SO_4$ were found under worst visibility conditions when the third haze occurred. These results suggested that the carbon components from the primary emission might be relatively important for the visibility reduction for this haze event.

Trajectory clustering analysis showed that the air quality in Suzhou was mostly affected by air masses originating from North and Southwestern areas which were associated with high aerosol concentrations. Distinct aerosol composition profiles, light extinction coefficients and species contributions to visibility reduction were observed when air masses originated from different directions, e.g. AS was the predominant contributor to light extinction for trajectories from north and northwest, while in other cases the light extinction was primarily affected by OM.

The likely sources of aerosol and the major species based on the PSCF method were mainly from local anthropogenic activities and source emissions transported from nearby cities. The northwestern to southern regions may be important sources of aerosols and the major components. The northern and northwestern areas were predominant source regions for sulfate, nitrate and ammonium aerosols, whereas the southern area could be the common source region for carbonaceous species. This information has the implications for the importance of collaborative air pollution control strategy in the Yangtze River Delta Region.

Acknowledgements

This work was supported by the National Natural Science Foundation of China projects (41403089, 41375123), the "Strategic Priority Research Program" of the Chinese Academy of Sciences (KJZD-EW-TZ-G06-04), and the State Environmental Protection Key Laboratory of Sources and Control of Air Pollution Complex (SCAPC201310).

References

Antony Chen, L. W., Doddridge, B. G., Dickerson, R. R., Chow, J. C., Mueller, P. K., Quinn, J., and Butler, W. A.: Seasonal variations in elemental carbon aerosol, carbon monoxide and sulfur dioxide: Implications for sources, Geophys. Res. Lett., 28, 1711-1714, doi: 10.1029/2000gl012354, 2001.

Arimoto, R., Duce, R. A., Savoie, D. L., Prospero, J. M., Talbot, R., Cullen, J. D., Tomza, U., Lewis, N. F., and Jay, B. J.: Relationships among aerosol constituents from Asia and the North Pacific during PEM-West A, J. Geophys. Res.-Atmos., 101, 2011-2023, doi: 10.1029/95jd01071, 1996.

Ashbaugh, L. L., Malm, W. C., and Sadeh, W. Z.: A residence time probability analysis of sulfur concentrations at Grand-Canyon-National-Park, Atmos. Environ., 19, 1263-1270, doi: 10.1016/0004-6981(85)90256-2, 1985.

Bae, M.-S., Schauer, J. J., DeMinter, J. T., Turner, J. R., Smith, D., and Cary, R. A.: Validation of a semi-continuous instrument for elemental carbon and organic carbon using a thermal-optical method, Atmos. Environ., 38, 2885-2893, doi: 10.1016/j.atmosenv.2004.02.027, 2004.

Castro, L. M., Pio, C. A., Harrison, R. M., and Smith, D. J. T.: Carbonaceous aerosol in urban and rural European atmospheres: estimation of secondary organic carbon concentrations, Atmos. Environ., 33, 2771-2781, doi: 10.1016/S1352-2310(98)00331-8, 1999.

Charlson, R. J., Lovelock, J. E., Andreae, M. O., and Warren, S. G.: Oceanic phytoplankton, atmospheric sulfur, cloud albedo and climate, Nature, 326, 655-661, doi: 10.1038/326655a0, 1987.

Chen, J., Zhao, C. S., Ma, N., Liu, P. F., Göbel, T., Hallbauer, E., Deng, Z. Z., Ran, L., Xu, W. Y., Liang, Z., Liu, H. J., Yan, P., Zhou, X. J., and Wiedensohler, A.: A parameterization of low visibilities for hazy days in the North China Plain, Atmos. Chem. Phys., 12, 4935-4950, doi: 10.5194/acp-12-4935-2012, 2012.

Chen, R., Zhao, Z., and Kan, H.: Heavy smog and hospital visits in Beijing, China, Am. J. Respir. Crit. Care Med., 188, 1170-1171, doi:

671 10.1164/rccm.201304-0678LE, 2013.
672 Chow, J. C., Doraiswamy, P., Watson, J. G., Antony-Chen, L. W., Ho, S. S. H., and
673 Sodeman, D. A.: Advances in integrated and continuous measurements for particle
674 mass and chemical, composition, J. Air Waste Manage. Assoc., 58, 141-163, doi:
675 10.3155/1047-3289.58.2.141, 2008.
676 Clegg, S. L., Brimblecombe, P., and Wexler, A. S.: Thermodynamic model of the
677 system H^+–NH_4^+–SO_4^{2-}–NO_3^-–H_2O at tropospheric temperatures, The Journal of
678 Physical Chemistry A, 102, 2137-2154, doi: 10.1021/jp973042r, 1998.
679 Ding, A. J., Fu, C. B., Yang, X. Q., Sun, J. N., Zheng, L. F., Xie, Y. N., Herrmann, E.,
680 Nie, W., Petaja, T., Kerminen, V. M., and Kulmala, M.: Ozone and fine particle in
681 the western Yangtze River Delta: an overview of 1 yr data at the SORPES station,
682 Atmos. Chem. Phys., 13, 5813-5830, doi: 10.5194/acp-13-5813-2013, 2013.
683 Fang, G. C., Chang, C. N., Wu, Y. S., Fu, P. P. C., Yang, C. J., Chen, C. D., and Chang,
684 S. C.: Ambient suspended particulate matters and related chemical species study in
685 central Taiwan, Taichung during 1998-2001, Atmos. Environ., 36, 1921-1928, doi:
686 10.1016/S1352-2310(02)00187-5, 2002.
687 Fu, Q., Zhuang, G., Wang, J., Xu, C., Huang, K., Li, J., Hou, B., Lu, T., and Streets, D.
688 G.: Mechanism of formation of the heaviest pollution episode ever recorded in the
689 Yangtze River Delta, China, Atmos. Environ., 42, 2023-2036, doi:
690 10.1016/j.atmosenv.2007.12.002, 2008.
691 Gao, J., Tian, H., Cheng, K., Lu, L., Zheng, M., Wang, S., Hao, J., Wang, K., Hua, S.,
692 Zhu, C., and Wang, Y.: The variation of chemical characteristics of $PM_{2.5}$ and PM_{10}
693 and formation causes during two haze pollution events in urban Beijing, China,
694 Atmos. Environ., 107, 1-8, doi: 10.1016/j.atmosenv.2015.02.022, 2015.
695 Han, S., Wu, J., Zhang, Y., Cai, Z., Feng, Y., Yao, Q., Li, X., Liu, Y., and Zhang, M.:
696 Characteristics and formation mechanism of a winter haze-fog episode in Tianjin,
697 China, Atmos. Environ., 98, 323-330, doi: 10.1016/j.atmosenv.2014.08.078, 2014.
698 He, K., Zhao, Q., Ma, Y., Duan, F., Yang, F., Shi, Z., and Chen, G.: Spatial and
699 seasonal variability of $PM_{2.5}$ acidity at two Chinese megacities: insights into the
700 formation of secondary inorganic aerosols, Atmos. Chem. Phys., 12, 1377-1395,

701 doi: 10.5194/acp-12-1377-2012, 2012.
702 Hewitt, C. N.: The atmospheric chemistry of sulphur and nitrogen in power station
703 plumes, Atmos. Environ., 35, 1155-1170, doi: 10.1016/S1352-2310(00)00463-5,
704 2001.
705 Hsu, Y. K., Holsen, T. M., and Hopke, P. K.: Comparison of hybrid receptor models to
706 locate PCB sources in Chicago, Atmos. Environ., 37, 545-562, doi:
707 10.1016/S1352-2310(02)00886-5, 2003.
708 Hu, M., He, L. Y., Zhang, Y. H., Wang, M., Kim, Y. P., and Moon, K. C.: Seasonal
709 variation of ionic species in fine particles at Qingdao, China, Atmos. Environ., 36,
710 5853-5859, doi: 10.1016/S1352-2310(02)00581-2, 2002a.
711 Hu, M., Zhou, F., Shao, K., Zhang, Y., Tang, X., and Slanina, J.: Diurnal variations of
712 aerosol chemical compositions and related gaseous pollutants in Beijing and
713 Guangzhou, J. Environ. Sci. Health A Tox. Hazard. Subst. Environ. Eng., 37,
714 479-488, doi: 10.1081/ese-120003229, 2002b.
715 Hua, W., Chen, Z. M., Jie, C. Y., Kondo, Y., Hofzumahaus, A., Takegawa, N., Chang,
716 C. C., Lu, K. D., Miyazaki, Y., Kita, K., Wang, H. L., Zhang, Y. H., and Hu, M.:
717 Atmospheric hydrogen peroxide and organic hydroperoxides during
718 PRIDE-PRD'06, China: their concentration, formation mechanism and contribution
719 to secondary aerosols, Atmos. Chem. Phys., 8, 6755-6773, doi:
720 10.5194/acp-8-6755-2008, 2008.
721 Huang, R. J., Zhang, Y., Bozzetti, C., Ho, K. F., Cao, J. J., Han, Y., Daellenbach, K. R.,
722 Slowik, J. G., Platt, S. M., Canonaco, F., Zotter, P., Wolf, R., Pieber, S. M., Bruns,
723 E. A., Crippa, M., Ciarelli, G., Piazzalunga, A., Schwikowski, M., Abbaszade, G.,
724 Schnelle-Kreis, J., Zimmermann, R., An, Z., Szidat, S., Baltensperger, U., El
725 Haddad, I., and Prevot, A. S.: High secondary aerosol contribution to particulate
726 pollution during haze events in China, Nature, 514, 218-222, doi:
727 10.1038/nature13774, 2014.
728 Jansen, R. C., Shi, Y., Chen, J., Hu, Y., Xu, C., Hong, S., Li, J., and Zhang, M.: Using
729 hourly measurements to explore the role of secondary inorganic aerosol in $PM_{2.5}$
730 during haze and fog in Hangzhou, China, Adv. Atmos. Sci., 31, 1427-1434, doi:

731 10.1007/s00376-014-4042-2, 2014.
732 Ji, D., Li, L., Wang, Y., Zhang, J., Cheng, M., Sun, Y., Liu, Z., Wang, L., Tang, G., Hu,
733 B., Chao, N., Wen, T., and Miao, H.: The heaviest particulate air-pollution episodes
734 occurred in northern China in January, 2013: Insights gained from observation,
735 Atmos. Environ., 92, 546-556, doi: 10.1016/j.atmosenv.2014.04.048, 2014.
736 Khoder, M. I.: Atmospheric conversion of sulfur dioxide to particulate sulfate and
737 nitrogen dioxide to particulate nitrate and gaseous nitric acid in an urban area,
738 Chemosphere, 49, 675-684, doi: 10.1016/S0045-6535(02)00391-0, 2002.
739 Li, W., Zhou, S., Wang, X., Xu, Z., Yuan, C., Yu, Y., Zhang, Q., and Wang, W.:
740 Integrated evaluation of aerosols from regional brown hazes over northern China in
741 winter: Concentrations, sources, transformation, and mixing states, J Geophys Res,
742 116, doi: 10.1029/2010jd015099, 2011.
743 Pathak, R. K., Wu, W. S., and Wang, T.: Summertime $PM_{2.5}$ ionic species in four
744 major cities of China: nitrate formation in an ammonia-deficient atmosphere,
745 Atmos. Chem. Phys., 9, 1711-1722, doi: 10.5194/acp-9-1711-2009, 2009.
746 Pathak, R. K., Wang, T., and Wu, W. S.: Nighttime enhancement of $PM_{2.5}$ nitrate in
747 ammonia-poor atmospheric conditions in Beijing and Shanghai: Plausible
748 contributions of heterogeneous hydrolysis of N_2O_5 and HNO_3 partitioning, Atmos.
749 Environ., 45, 1183-1191, doi: 10.1016/j.atmosenv.2010.09.003, 2011.
750 Pitchford, M., Maim, W., Schichtel, B., Kumar, N., Lowenthal, D., and Hand, J.:
751 Revised algorithm for estimating light extinction from IMPROVE particle
752 speciation data, J. Air Waste Manage. Assoc., 57, 1326-1336, doi:
753 10.3155/1047-3289.57.11.1326, 2007.
754 Polissar, A. V., Hopke, P. K., Paatero, P., Kaufmann, Y. J., Hall, D. K., Bodhaine, B.
755 A., Dutton, E. G., and Harris, J. M.: The aerosol at Barrow, Alaska: long-term
756 trends and source locations, Atmos. Environ., 33, 2441-2458, doi:
757 10.1016/S1352-2310(98)00423-3, 1999.
758 Quan, J., Tie, X., Zhang, Q., Liu, Q., Li, X., Gao, Y., and Zhao, D.: Characteristics of
759 heavy aerosol pollution during the 2012–2013 winter in Beijing, China, Atmos.
760 Environ., 88, 83-89, doi: 10.1016/j.atmosenv.2014.01.058, 2014.

761 Ramanathan, V., and Vogelmann, A. M.: Greenhouse effect, atmospheric solar
762 absorption and the Earth's radiation budget: From the Arrhenius-Langley era to the
763 1990s, Ambio, 26, 38-46, 1997.
764 Seinfeld, J. H., and Pandis, S. N.: Atmospheric Chemistry and Physics: From Air
765 Pollution to Climate Change, Second ed., John Wiley & Sons, Hoboken, New
766 Jersey, 2012.
767 Sun, Y., Zhuang, G., Tang, A., Wang, Y., and An, Z.: Chemical Characteristics of
768 $PM_{2.5}$ and PM_{10} in Haze−Fog Episodes in Beijing, Environ. Sci. Technol., 40,
769 3148-3155, doi: 10.1021/es051533g, 2006.
770 Sun, Y., Jiang, Q., Wang, Z., Fu, P., Li, J., Yang, T., and Yin, Y.: Investigation of the
771 sources and evolution processes of severe haze pollution in Beijing in January
772 2013, J. Geophys. Res.: Atmos., 119, 4380-4398, doi: 10.1002/2014jd021641,
773 2014.
774 Sun, Y. L., Zhang, Q., Schwab, J. J., Chen, W. N., Bae, M. S., Lin, Y. C., Hung, H. M.,
775 and Demerjian, K. L.: A case study of aerosol processing and evolution in summer
776 in New York City, Atmos. Chem. Phys., 11, 12737-12750, doi:
777 10.5194/acp-11-12737-2011, 2011.
778 Sun, Y. L., Wang, Z. F., Fu, P. Q., Jiang, Q., Yang, T., Li, J., and Ge, X. L.: The impact
779 of relative humidity on aerosol composition and evolution processes during
780 wintertime in Beijing, China, Atmos. Environ., 77, 927-934, doi:
781 10.1016/j.atmosenv.2013.06.019, 2013a.
782 Sun, Y. L., Wang, Z. F., Fu, P. Q., Yang, T., Jiang, Q., Dong, H. B., Li, J., and Jia, J. J.:
783 Aerosol composition, sources and processes during wintertime in Beijing, China,
784 Atmos. Chem. Phys., 13, 4577-4592, doi: 10.5194/acp-13-4577-2013, 2013b.
785 Tan, J., Duan, J., He, K., Ma, Y., Duan, F., Chen, Y., and Fu, J.: Chemical
786 characteristics of $PM_{2.5}$ during a typical haze episode in Guangzhou, J. Environ.
787 Sci., 21, 774-781, doi: 10.1016/s1001-0742(08)62340-2, 2009.
788 Tao, J., Zhang, L. M., Ho, K. F., Zhang, R. J., Lin, Z. J., Zhang, Z. S., Lin, M., Cao, J.
789 J., Liu, S. X., and Wang, G. H.: Impact of $PM_{2.5}$ chemical compositions on aerosol
790 light scattering in Guangzhou - the largest megacity in South China, Atmos. Res.,

135, 48-58, doi: 10.1016/j.atmosres.2013.08.015, 2014.

Tao, J., Zhang, L., Gao, J., Wang, H., Chai, F., and Wang, S.: Aerosol chemical composition and light scattering during a winter season in Beijing, Atmos. Environ., 110, 36-44, doi: 10.1016/j.atmosenv.2015.03.037, 2015.

Tegen, I., Koch, D., Lacis, A. A., and Sato, M.: Trends in tropospheric aerosol loads and corresponding impact on direct radiative forcing between 1950 and 1990: A model study, J. Geophys. Res.-Atmos., 105, 26971-26989, doi: 10.1029/2000jd900280, 2000.

Tie, X., Madronich, S., Li, G., Ying, Z., Weinheimer, A., Apel, E., and Campos, T.: Simulation of Mexico City plumes during the MIRAGE-Mex field campaign using the WRF-Chem model, Atmos. Chem. Phys., 9, 4621-4638, doi: 10.5194/acp-9-4621-2009, 2009a.

Tie, X., Wu, D., and Brasseur, G.: Lung cancer mortality and exposure to atmospheric aerosol particles in Guangzhou, China, Atmos. Environ., 43, 2375-2377, doi: 10.1016/j.atmosenv.2009.01.036, 2009b.

Trebs, I., Meixner, F. X., Slanina, J., Otjes, R., Jongejan, P., and Andreae, M. O.: Real-time measurements of ammonia, acidic trace gases and water-soluble inorganic aerosol species at a rural site in the Amazon Basin, Atmos. Chem. Phys., 4, 967-987, doi: 10.5194/acp-4-967-2004, 2004.

Wang, H., An, J., Shen, L., Zhu, B., Pan, C., Liu, Z., Liu, X., Duan, Q., Liu, X., and Wang, Y.: Mechanism for the formation and microphysical characteristics of submicron aerosol during heavy haze pollution episode in the Yangtze River Delta, China, Sci. Total Environ., 490, 501-508, doi: 10.1016/j.scitotenv.2014.05.009, 2014a.

Wang, H., Xu, J., Zhang, M., Yang, Y., Shen, X., Wang, Y., Chen, D., and Guo, J.: A study of the meteorological causes of a prolonged and severe haze episode in January 2013 over central-eastern China, Atmos. Environ., 98, 146-157, doi: 10.1016/j.atmosenv.2014.08.053, 2014b.

Wang, J., Wang, S., Jiang, J., Ding, A., Zheng, M., Zhao, B., Wong, D. C., Zhou, W., Zheng, G., Wang, L., Pleim, J. E., and Hao, J.: Impact of aerosol-meteorology

821 interactions on fine particle pollution during China's severe haze episode in
822 January 2013, Environ. Res. Lett., 9, doi: 10.1088/1748-9326/9/9/094002, 2014c.
823 Wang, Y., Zhuang, G. S., Tang, A. H., Yuan, H., Sun, Y. L., Chen, S. A., and Zheng, A.
824 H.: The ion chemistry and the source of $PM_{2.5}$ aerosol in Beijing, Atmos. Environ.,
825 39, 3771-3784, doi: 10.1016/j.atmosenv.2005.03.013, 2005.
826 Wang, Y., Zhuang, G., Sun, Y., and An, Z.: The variation of characteristics and
827 formation mechanisms of aerosols in dust, haze, and clear days in Beijing, Atmos.
828 Environ., 40, 6579-6591, doi: 10.1016/j.atmosenv.2006.05.066, 2006.
829 Wang, Y., Yao, L., Wang, L., Liu, Z., Ji, D., Tang, G., Zhang, J., Sun, Y., Hu, B., and
830 Xin, J.: Mechanism for the formation of the January 2013 heavy haze pollution
831 episode over central and eastern China, Sci. China-Earth Sci., 57, 14-25, doi:
832 10.1007/s11430-013-4773-4, 2014d.
833 Wang, Y. H., Liu, Z. R., Zhang, J. K., Hu, B., Ji, D. S., Yu, Y. C., and Wang, Y. S.:
834 Aerosol physicochemical properties and implications for visibility during an
835 intense haze episode during winter in Beijing, Atmos. Chem. Phys., 15, 3205-3215,
836 doi: 10.5194/acp-15-3205-2015, 2015.
837 Wang, Y. Q., Zhang, X. Y., and Draxler, R. R.: TrajStat: GIS-based software that uses
838 various trajectory statistical analysis methods to identify potential sources from
839 long-term air pollution measurement data, Environ. Modell. Softw., 24, 938-939,
840 doi: 10.1016/j.envsoft.2009.01.004, 2009.
841 Warneck, P.: Chemistry of the natural atmosphere, Academic press, 1999.
842 Wehner, B., Birmili, W., Ditas, F., Wu, Z., Hu, M., Liu, X., Mao, J., Sugimoto, N., and
843 Wiedensohler, A.: Relationships between submicrometer particulate air pollution
844 and air mass history in Beijing, China, 2004-2006, Atmos. Chem. Phys., 8,
845 6155-6168, doi: 10.5194/acp-8-6155-2008, 2008.
846 Xiao, H. Y., and Liu, C. Q.: Chemical characteristics of water-soluble components in
847 TSP over Guiyang, SW China, 2003, Atmos. Environ., 38, 6297-6306, doi:
848 10.1016/j.atmosenv.2004.08.033, 2004.
849 Yang, F. M., He, K. B., Ma, Y. L., Zhang, Q., Cadle, S. H., Chan, T., and Mulawa, P.
850 A.: Characterization of carbonaceous species of ambient $PM_{2.5}$ in Beijing, China, J.

851 Air Waste Manage. Assoc., 55, 984-992, doi: 10.1080/10473289.2005.10464699,
852 2005.
853 Yang, Y., Liu, X., Qu, Y., Wang, J., An, J., Zhang, Y., and Zhang, F.: Formation
854 mechanism of continuous extreme haze episodes in the megacity Beijing, China, in
855 January 2013, Atmos. Res., 155, 192-203, doi: 10.1016/j.atmosres.2014.11.023,
856 2015.
857 Yao, X. H., Chan, C. K., Fang, M., Cadle, S., Chan, T., Mulawa, P., He, K. B., and Ye,
858 B. M.: The water-soluble ionic composition of $PM_{2.5}$ in Shanghai and Beijing,
859 China, Atmos. Environ., 36, 4223-4234, doi: 10.1016/S1352-2310(02)00342-4,
860 2002.
861 Yu, H. B., Liu, S. C., and Dickinson, R. E.: Radiative effects of aerosols on the
862 evolution of the atmospheric boundary layer, J. Geophys. Res.-Atmos., 107, AAC
863 3-1–AAC 3-14, doi: 10.1029/2001jd000754, 2002.
864 Yu, S., Zhang, Q., Yan, R., Wang, S., Li, P., Chen, B., Liu, W., and Zhang, X.: Origin
865 of air pollution during a weekly heavy haze episode in Hangzhou, China, Environ.
866 Chem. Lett., 12, 543-550, doi: 10.1007/s10311-014-0483-1, 2014.
867 Zhang, J., Chen, J., Yang, L., Sui, X., Yao, L., Zheng, L., Wen, L., Xu, C., and Wang,
868 W.: Indoor $PM_{2.5}$ and its chemical composition during a heavy haze-fog episode at
869 Jinan, China, Atmos. Environ., 99, 641-649, doi: 10.1016/j.atmosenv.2014.10.026,
870 2014.
871 Zhang, Q., Quan, J., Tie, X., Li, X., Liu, Q., Gao, Y., and Zhao, D.: Effects of
872 meteorology and secondary particle formation on visibility during heavy haze
873 events in Beijing, China, Sci. Total Environ., 502, 578-584, doi:
874 10.1016/j.scitotenv.2014.09.079, 2015.
875 Zhang, X. Y., Wang, Y. Q., Niu, T., Zhang, X. C., Gong, S. L., Zhang, Y. M., and Sun,
876 J. Y.: Atmospheric aerosol compositions in China: spatial/temporal variability,
877 chemical signature, regional haze distribution and comparisons with global
878 aerosols, Atmos. Chem. Phys., 12, 779-799, doi: 10.5194/acp-12-779-2012, 2012.
879 Zhao, X. J., Zhao, P. S., Xu, J., Meng, W., Pu, W. W., Dong, F., He, D., and Shi, Q. F.:
880 Analysis of a winter regional haze event and its formation mechanism in the North

881 China Plain, Atmos. Chem. Phys., 13, 5685-5696, doi: 10.5194/acp-13-5685-2013,
882 2013.
883 Zheng, G. J., Duan, F. K., Su, H., Ma, Y. L., Cheng, Y., Zheng, B., Zhang, Q., Huang,
884 T., Kimoto, T., Chang, D., Poeschl, U., Cheng, Y. F., and He, K. B.: Exploring the
885 severe winter haze in Beijing: the impact of synoptic weather, regional transport
886 and heterogeneous reactions, Atmos. Chem. Phys., 15, 2969-2983, doi:
887 10.5194/acp-15-2969-2015, 2015.
888
889

890 Table 1. The percentages of air masses from each trajectory cluster and associated
891 mean concentrations (μg m^{-3}) of $PM_{2.5}$ and its major chemical components, and mean
892 b_{ext} (Mm^{-1}).

	1	2	3	4	5	6
Percent (%)	20.6	31.7	20.6	12.7	6.3	7.9
$PM_{2.5}$	129	117	167	103	84.0	87.4
OC	21.1	22.8	25.3	16.4	30.5	20.3
EC	2.05	3.87	2.21	1.45	3.90	1.86
Sulfate	22.9	18.2	32.4	23.1	8.85	8.39
Nitrate	11.5	10.0	16.9	7.84	3.26	7.91
Ammonium	15.2	12.3	18.9	12.4	7.93	9.88
b_{ext}	675	597	921	556	548	463

893
894

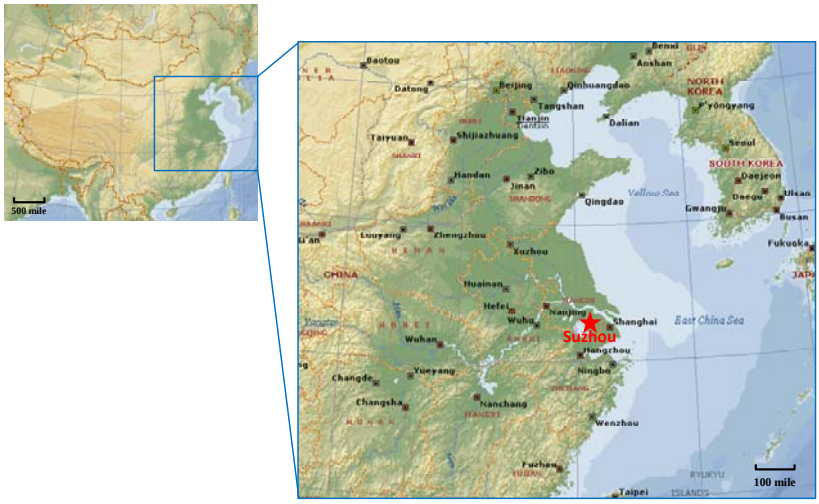

Figure 1. The sampling site in Suzhou. The locations of major cities with a population of more than 1 million (such as Qingdao, Nanjing and Hangzhou) are marked with a square symbol. The topographical map was derived from Microsoft® Encarta® 2009 © 1993 - 2008.

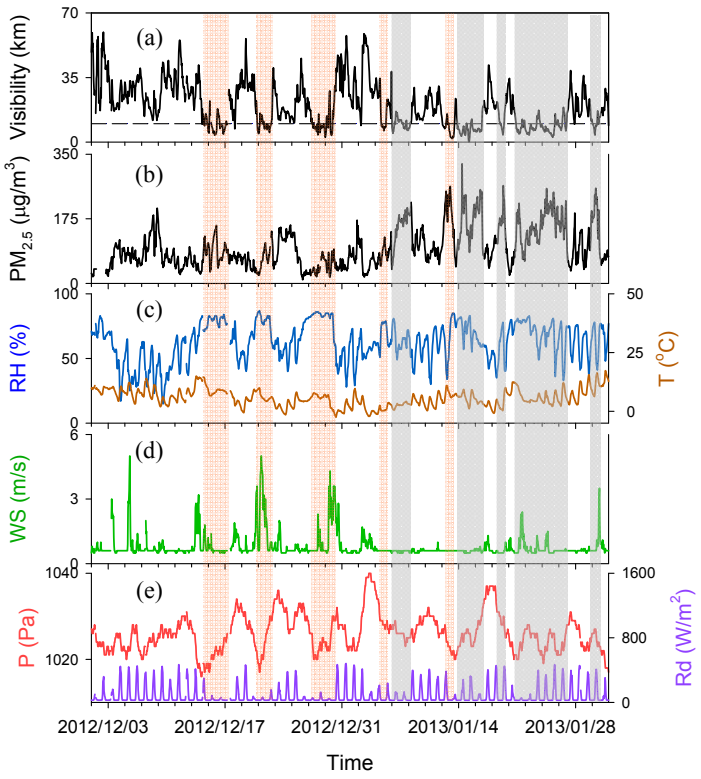

Figure 2. Time series of (a) visibility; (b) $PM_{2.5}$ concentration; (c) relative humidity (RH) and temperature (T); (d) wind speed (WS) and pressure (P); and (e) solar radiation (Rd). The shaded areas in orange represent periods when visibility were

lower than 10 km and accompanied by precipitation. The shaded areas in grey represent haze periods.

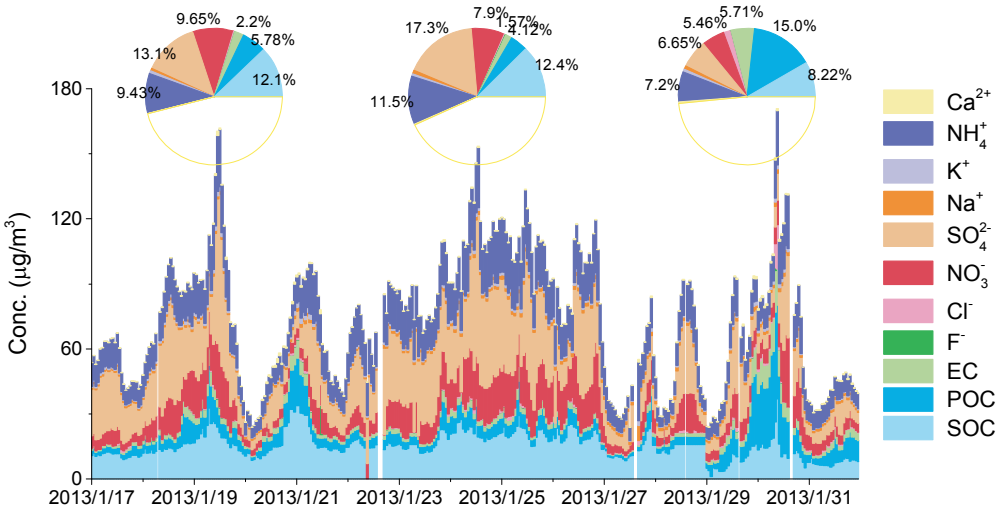

Figure 3. Temporal distribution of water soluble inorganic ions and carbonaceous species. The aerosol composition in the three haze events was also illustrated in the pie chart.

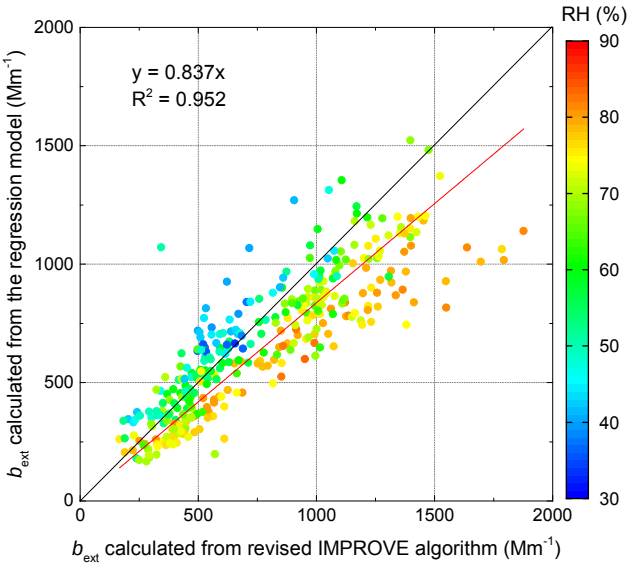

Figure 4. Comparison of the calculated b_{ext} between those obtained from the regression equation and those from the IMPROVE algorithm.

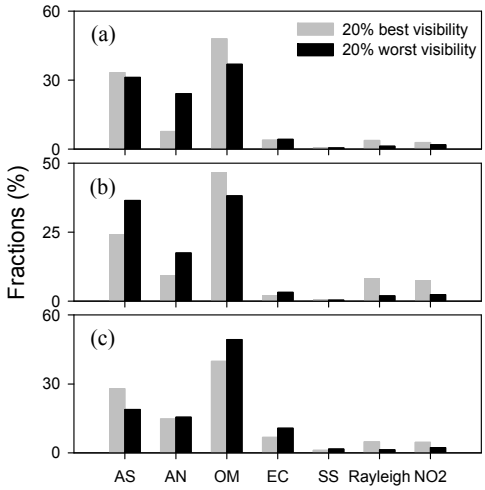

Figure 5. Relative contributions of various chemical components in $PM_{2.5}$ (ammonium sulfate (AS), ammonium nitrate (AN), OM, and EC) to the total light extinction under 20% best and 20% worst visibility conditions during the first (a), second (b), and third (c) haze events.

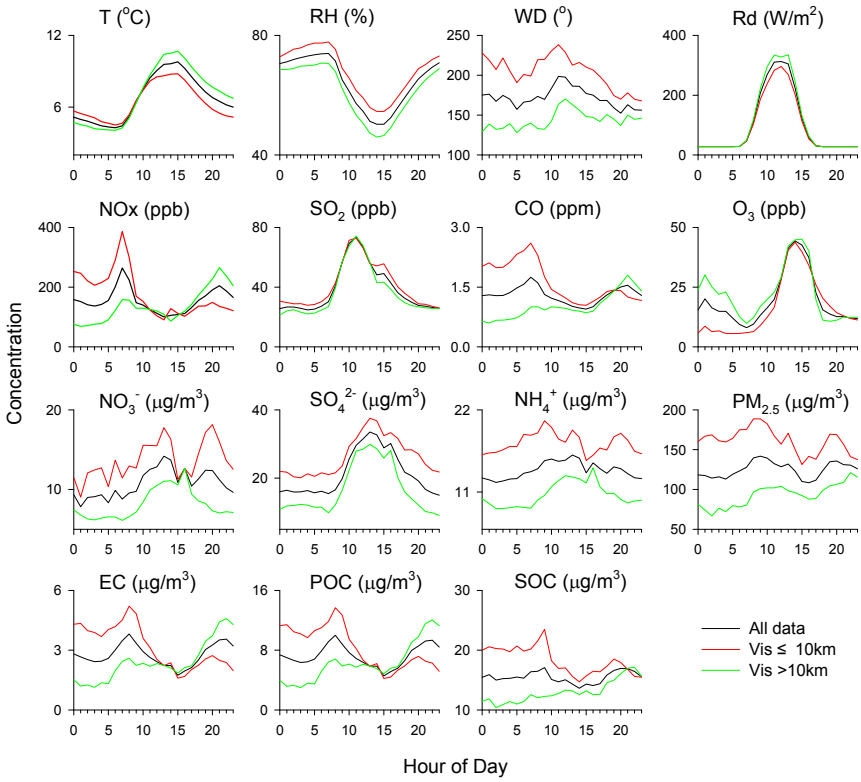

Figure 6. Diurnal profiles of meteorological variables, aerosol precursors (NO_X, SO_2), CO, O_3, $PM_{2.5}$, and major aerosol compounds (NO_3^-, SO_4^{2-}, NH_4^+, EC, POC, SOC)

under different visibility conditions.

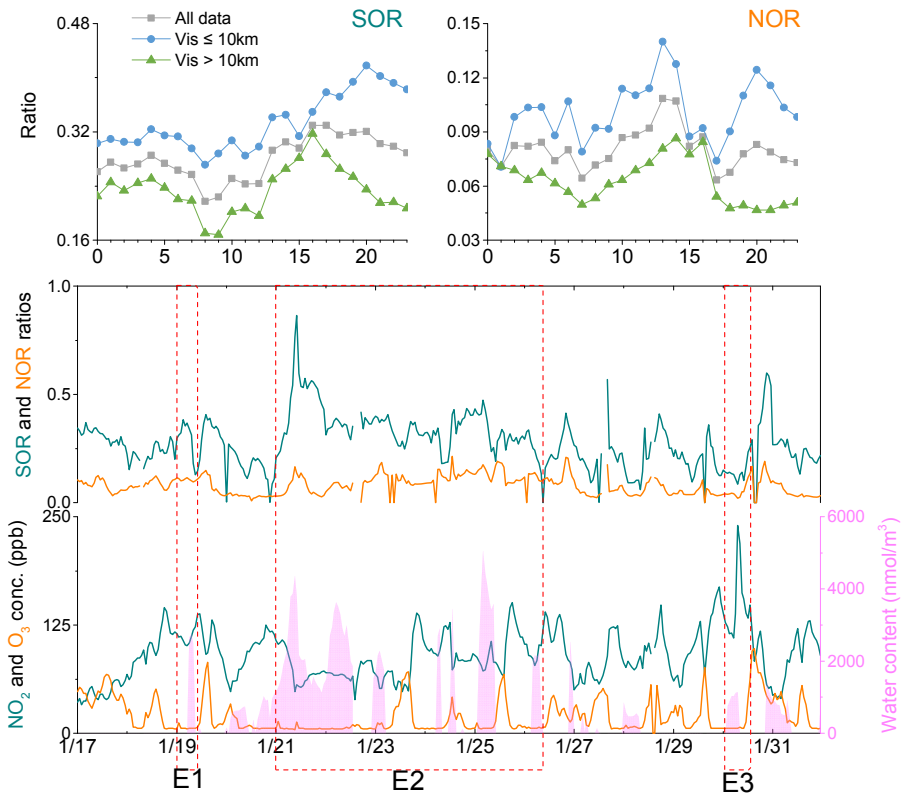

Figure 7. Temporary distributions of SOR, NOR, NO_2, O_3 and aerosol water content. Diurnal profiles of NOR and SOR ratios under different visibility conditions.

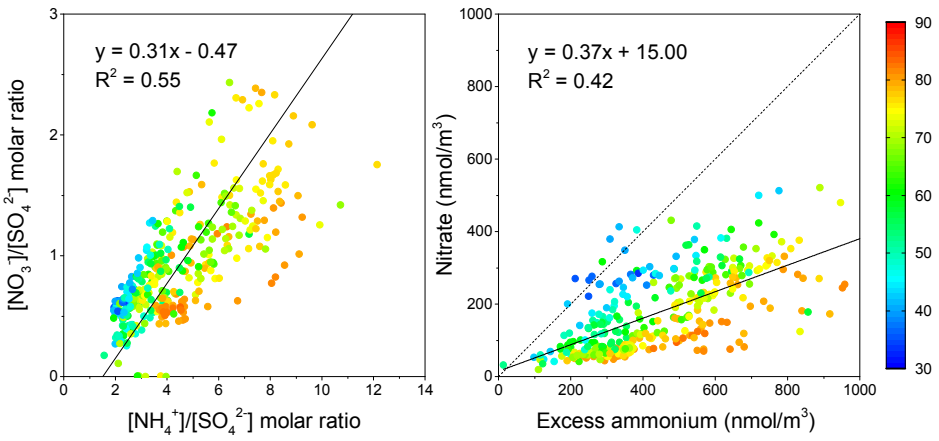

Figure 8. Nitrate to sulfate molar ratio as a function of ammonium to sulfate molar ratio (left) and relationship between molar concentrations of nitrate and excess

ammonium (right).

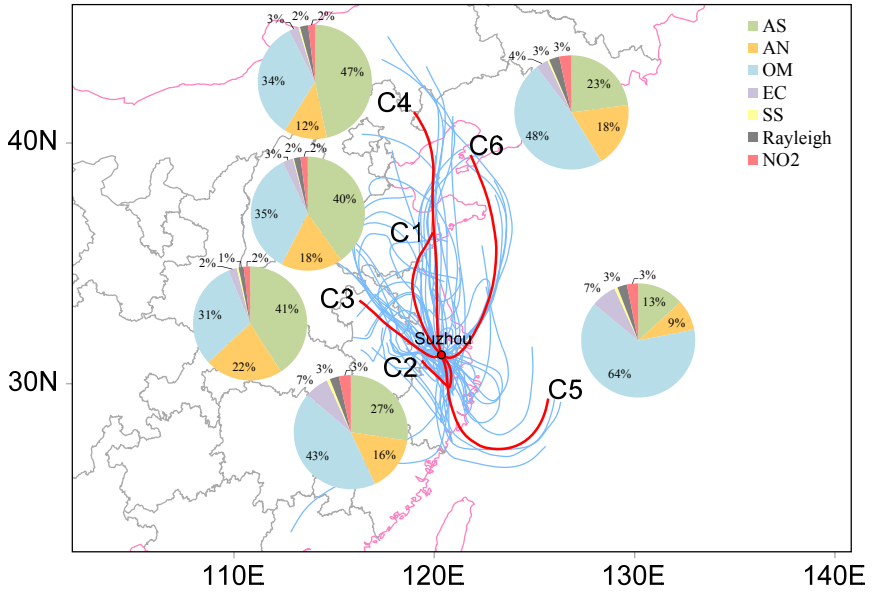

Figure 9. Backward air mass trajectories and six mean trajectories after the cluster analysis at the sampling site during Jan. 17 to 31. Relative contributions of various chemical components to the total light extinction in different clusters are illustrated.

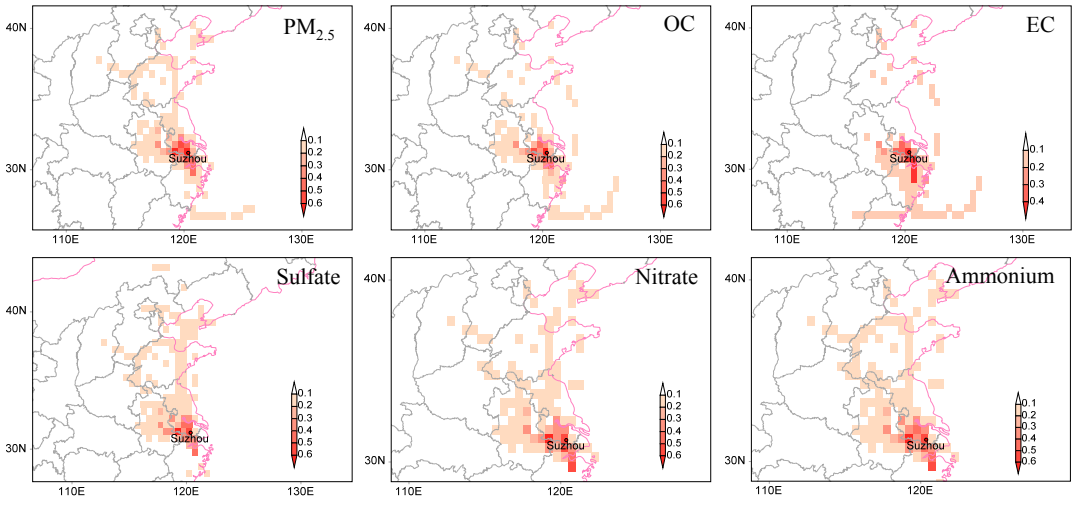

Figure 10. The PSCF maps for $PM_{2.5}$, OC, EC, sulfate, nitrate, and ammonium.